Neuron
Article

Closing In on the Resting State of the Shaker K^+ Channel

Medha M. Pathak,[1,8,9] Vladimir Yarov-Yarovoy,[4,8] Gautam Agarwal,[2] Benoît Roux,[6] Patrick Barth,[5] Susy Kohout,[3] Francesco Tombola,[3] and Ehud Y. Isacoff[1,2,3,7,*]
[1]Biophysics Graduate Program
[2]Neuroscience Graduate Program
[3]Department of Molecular and Cell Biology
University of California, Berkeley, Berkeley, CA 94720, USA
[4]Department of Pharmacology
[5]Department of Biochemistry
University of Washington, Seattle, WA 98195, USA
[6]Institute of Molecular Pediatrics Science and Department of Biochemistry and Molecular Biology, University of Chicago, Chicago, IL 60637, USA
[7]Physical Bioscience and Material Science Divisions, Lawrence Berkeley National Laboratory, Berkeley, CA 94720, USA
[8]These authors contributed equally to this work.
[9]Present address: Department of Neurobiology, Harvard Medical School, Boston, MA 02115.
*Correspondence: ehud@berkeley.edu
DOI 10.1016/j.neuron.2007.09.023

SUMMARY

Membrane depolarization causes voltage-gated ion channels to transition from a resting/closed conformation to an activated/open conformation. We used voltage-clamp fluorometry to measure protein motion at specific regions of the Shaker Kv channel. This enabled us to construct new structural models of the resting/closed and activated/open states based on the Kv1.2 crystal structure using the Rosetta-Membrane method and molecular dynamics simulations. Our models account for the measured gating charge displacement and suggest a molecular mechanism of activation in which the primary voltage sensors, S4s, rotate by ~180° as they move "outward" by 6–8 Å. A subsequent tilting motion of the S4s and the pore domain helices, S5s, of all four subunits induces a concerted movement of the channel's S4-S5 linkers and S6 helices, allowing ion conduction. Our models are compatible with a wide body of data and resolve apparent contradictions that previously led to several distinct models of voltage sensing.

INTRODUCTION

Voltage-gated ion channels open and close in response to changes in membrane potential and rapidly and selectively conduct ions selectively across cell membranes. Their ability to sense the membrane potential is conferred via a voltage-sensing domain (VSD, transmembrane segments S1-S4), which regulates the conformation of molecular gates located in the pore domain (PD, transmembrane segments S5-S6). Detailed structural information at atomic resolution is needed to understand the mechanism underlying voltage gating. The recent structure of the mammalian Kv1.2 voltage-gated K^+ channel, though partially incomplete, revealed the general organization of the VSD in what appears to be the activated and open state (Long et al., 2005a). The earlier high-resolution crystal structure of the bacterial voltage-gated channel KvAP (Jiang et al., 2003a, 2003b) captured the protein in a nonnative conformation (Lee et al., 2005), with the VSDs separated from the PD, suggesting that the interactions between the VSD and PD are weak and that large relative movements could occur between these two domains during gating.

To understand the voltage-sensing motion, recent studies tried to elucidate the resting/closed conformation by measuring voltage-dependent changes in internal and external accessibility of VSD segments (Gandhi et al., 2003; Phillips et al., 2005; Ruta et al., 2005), changes in the location of the charged S4 relative to either a pore blocker or to lipid-soluble probes (Chanda et al., 2005; Posson et al., 2005), and the distance needed to move an S4 charge through the membrane electric field (Ahern and Horn, 2005). These studies arrived at widely different models of the voltage-sensing motion (Tombola et al., 2005a). Two more recent studies—one that mapped the omega current pathway that ions take through the VSD in the resting state (Tombola et al., 2007) and the other which probed suppressor interactions between mutations in S4 and neighboring helices (Grabe et al., 2007)–arrived at more compatible results, but still lacked sufficient constraint for a complete model.

In order to fill in this gap, we performed a scan for protein motion on the externally accessible portion of the Shaker K^+ channel using voltage-clamp fluorometry

(VCF). VCF is a time-resolved method that provides information about local protein motion associated with specific gating steps. The structural rearrangement is reported by a fluorophore attached in a site-directed manner to one of a large series of individual positions from which one can reconstruct global motions. The VCF experiments provide new information on the VSD motion associated with activation, enabling us to construct new structural models of the resting and open state of the Kv1.2 channel. The models are generated by a combination of Rosetta-Membrane modeling and molecular dynamics simulations. The structural models are consistent with a number of key experimental observations and for the first time reconcile seemingly disparate data that have led to considerable debate in the field. Therefore, the findings provide new insight into the molecular mechanism of voltage-dependent gating.

RESULTS

Fluorescence Scan of the Voltage-Sensing Domain and the Pore Domain

We examined a large portion of the extracellular region of the Shaker channel and created rearrangement maps for the VSD and PD. Single amino acids were substituted with cysteine at 82 positions in the external portion of the channel (Figure 1 and Table 1). Of these cysteine mutants, 73 expressed functional channels and were studied further. Oocytes expressing each cysteine mutant were covalently labeled with the environment-sensitive fluorophore tetramethylrhodamine-6-maleimide (TMRM), which attached to the engineered cysteine. A single depolarizing voltage step from a holding potential of −80 mV to a positive voltage was used to activate and open the channel. The step was long enough to induce activation, opening and slow inactivation, resulting in a transient ionic current (Figure 1B). In parallel to measuring ionic current, we measured fluorescence from ~15% of the surface of the oocyte. A change in fluorescence (ΔF) was detected at 56 attachment positions, indicating that they are exposed enough to the external solution to permit conjugation by the charged extracellular TMRM and that a protein motion occurs in the labeled segment, or its surround, resulting in a change in the environment of the fluorophore. An examination of the ΔFs from all of the sites shows that they have unique fluorescence signatures, even in adjacent amino acid positions (Figure 1C and Table 1). This indicates that TMRM senses a small region of space in the vicinity of the side chain to which it is attached and that moving the attachment site by only one amino acid means pointing in a different direction where distinct interactions occur with the surrounding environment. In other words, VCF provides information about protein motion at a single amino acid resolution.

The ΔFs detected from different attachment sites varied in magnitude and polarity and tracked distinct subsets of functional transitions, such as activation, opening, inactivation, and recovery from inactivation. The ΔF measured during a depolarizing step could be divided into fast and slow components (Figure 1C). The slow component tracked the process of slow inactivation of the ionic current (data not shown, see Gandhi et al., 2000). In this study, we focus on the fast component, which took place during the rise of the ionic current and which we found to correspond to channel activation.

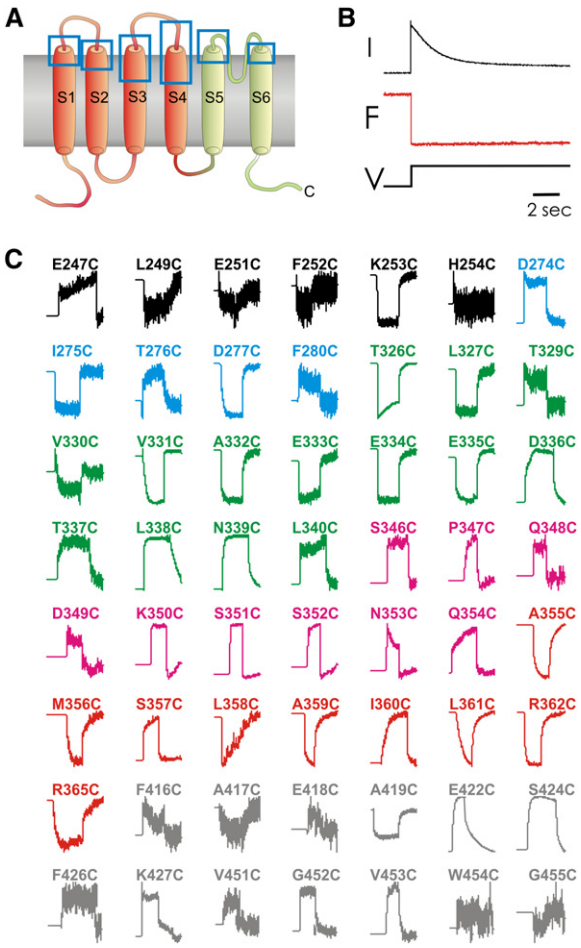

Figure 1. Fluorescence Scan Data Set

(A) Schematic diagram marking the regions of the Shaker channel included in the fluorescence scan. One subunit of the channel is shown, with the VSD in orange and the PD in green. Blue boxes mark the regions included in the fluorescence scan.

(B) Voltage step from a holding potential of −80 mV to a voltage between 0 and 50 mV for several seconds (V) opens the channel and slow inactivates it (I) while eliciting a fluorescence change from TMRM attached to the channel (F). At the site shown, TMRM fluorescence only tracks activation, not the process of slow inactivation.

(C) Fluorescence reports from the 56 positions at which ΔFs were detected. Each trace represents the mean of traces from three cells. The position of attachment of the fluorophore is indicated by a label on the top of each trace, with the following color scheme for labels: black, S1; blue, S2; green, S3; magenta, S3-S4; red, S4; gray, pore domain. The pre-step duration shown for each trace is 4 s and serves as the scale bar.

Table 1. Fluorescence Data Set

	Region	Shaker Residue	Kv1.2 Residue	Mean ΔF	Standard Deviation	Standard Error	n	Max ΔF
1	S1	E247	E183	0.00164	0.00067	0.00038	3	0.00241
2	S1	L249	L185	−0.00178	0.00089	0.00031	8	−0.00311
3	S1	E251	I187	0.00423	0.0053	0.002	7	0.01584
4	S1	F252	F188	−0.00127	0.00107	0.00038	8	0.00288
5	S1	K253	R189	−0.01351	0.00833	0.00315	7	−0.02918
6	S1	H254	D190	0.0037	0.00248	0.00111	5	0.00692
7	S2	D274	S217	0.00935	0.00566	0.00214	7	0.02172
8	S2	I275	F218	−0.01685	0.01039	0.00465	5	−0.03017
9	S2	T276	T219	0.00142	0.00071	0.00036	4	0.00222
10	S2	D277	D220	−0.00355	0.00164	0.00062	7	−0.00505
11	S2	F280	F223	0.0148	0.01648	0.00521	10	0.05425
12	S3	T326	T269	−0.02076	0.01267	0.00448	8	−0.04094
13	S3	L327	L270	−0.00265	0.00109	0.00044	6	−0.00386
14	S3	T329	T272	0.00388	0.00024	0.00012	4	0.00411
15	S3	V330	E273	0.00579	0.00489	0.00219	5	0.01423
16	S3	V331	L274	0.00807	0.00572	0.00256	5	0.01248
17	S3	A332	A275	−0.01797	0.01107	0.00418	7	−0.03487
18	S3	E333	E276	−0.00814	0.00837	0.00342	6	−0.02489
19	S3	E334	K277	−0.0258	0.0194	0.00792	6	−0.06302
20	S3	E335	P278	−0.00767	0.00358	0.00207	3	−0.01033
21	S3-S4	D336		0.00696	0.00586	0.00339	3	0.01272
22	S3-S4	T337		0.02245	0.02109	0.01055	4	0.04326
23	S3-S4	L338		0.02325	0.01153	0.00471	6	0.04184
24	S3-S4	N339		0.04264	0.02223	0.01112	4	0.07384
25	S3-S4	L340		0.00453	0.0011	0.00064	3	0.00579
26	S3-S4	S346*		0.01239	0.00615	0.00275	5	0.02
27	S3-S4	P347*	E279	0.00679	0.00434	0.00194	5	0.01044
28	S3-S4	Q348*	D280	0.0234	0.01207	0.00493	6	0.04108
29	S3-S4	D349*	A281	0.00546	0.00228	0.00114	4	0.00809
30	S3-S4	K350*	Q282	0.01705	0.00775	0.00258	9	0.02829
31	S3-S4	S351*	Q283	0.0703	0.02181	0.0069	10	0.1154
32	S3-S4	S352*	G284	0.02089	0.0088	0.00359	6	0.03135
33	S3-S4	N353*	Q285	0.04482	0.02435	0.00921	7	0.07764
34	S3-S4	Q354	Q286	0.03495	0.02354	0.00832	8	0.08101
35	S4	A355*	A287	−0.02414	0.01365	0.00483	8	−0.04552
36	S4	M356*	M288	−0.0161	0.0079	0.00354	5	−0.02187
37	S4	S357	S289	0.00918	0.00751	0.00306	6	0.02067
38	S4	L358*	L290	−0.01899	0.00616	0.00252	6	−0.02892
39	S4	A359*	A291	−0.02654	0.01974	0.00547	13	−0.06753
40	S4	I360*	I292	−0.003	0.00626	0.00313	4	−0.01114
41	S4	L361*	L293	−0.00075	0.00355	0.00145	6	−0.00458

Table 1. *Continued*

	Region	Shaker Residue	Kv1.2 Residue	Mean ΔF	Standard Deviation	Standard Error	n	Max ΔF
42	S4	R362*	R294	−0.04178	0.01476	0.0066	5	−0.0658
43	S4	R365*	R297	−0.01287	0.01037	0.00464	5	−0.03082
44	S5	F416	F348	0.00157	0.00044	0.00018	6	0.00214
45	S5	A417*	A349	−0.00229	0.00235	0.00118	4	−0.00572
46	S5	E418*	E350	0.0414	0.02247	0.00917	6	0.06231
47	P	A419*	A351	−0.06475	0.07468	0.04312	3	−0.1508
48	P	E422*	R354	0.08361	0.04435	0.01676	7	0.1359
49	P	S424*	S356	0.03267	0.02596	0.01161	5	0.07009
50	P	F426*	F358	0.00582	0.00245	0.00173	2	0.00756
51	P	K427	P359	0.01724	0.01064	0.00284	14	0.03765
52	P	V451	T383	0.0007	0.00075	0.00027	8	0.00168
53	P	G452	T384	0.01661	0.01129	0.00292	15	0.03591
54	S6	V453	I385	0.00434	0.00394	0.00149	7	0.00998
55	S6	W454	386	0.00071	0.0004	0.00023	3	0.00117
56	S6	G455*	G387	−0.00366	0.00242	0.0014	3	−0.00581

We did not observe fluorescence changes at positions F244 (F180), C245 (C181), or L246 (L182) in S1; F279 (F222), L281 (I224), or I282 (V225) in S2; F324 (F267), I325 (I268), or A328 (G271) in S3; V363 (V295), I364 (I296), L366 (L298), V367 (V299), or V369 (V301) in S4; F425 (Q357), S428 (S360), or A432 (A364) in the pore loop regions. We did not obtain expression of the cysteine mutants at T248 (T184) or P250 (P186) in S1; P278 (P221) or E283 (E226) in S2; G420 (D352), N423 (D355), P430 (P362), K456 (K388), or I457 (I389) in the pore domain. For sites marked with * the data were taken from experiments reported in Gandhi et al. (2000). For details on how the ΔF values were computed, please see Supplemental Experimental Procedures, section Data Analysis, Evaluating parameters for sites.

Detection of Protein Motion Associated with Voltage Sensing

Sites with a fast ΔF could experience an environment change during either the voltage-sensing steps of activation or during opening. We identified the positions that report on the voltage-sensing steps of activation by examining the ΔF elicited in response to a voltage step that changes the activation state but does not open the channel. For example, channels were given hyperpolarizing steps and depolarizing steps that were too small to open the channel, from a holding potential of −80 mV (Figure 2A). We observed ΔFs in response to these nonopening voltage steps for all of the sites in the VSD. Previous studies showed that the ΔF of TMRM at sites in or near the Shaker S4 segment tracks the channel's gating charge movement, i.e., the voltage-sensing steps of activation (Baker et al., 1998; Cha and Bezanilla, 1997; Gandhi et al., 2000; Mannuzzu and Isacoff, 2000; Mannuzzu et al., 1996). We found the same to be true for other sites in the VSD outside of S4. An example of this is shown for site 275 in S2, for which we compared the gating charge displaced to the ΔF (Figures 2B and 2C). We found that the kinetics of the ΔF tracked the ON and OFF gating current. Moreover, the steady-state voltage dependence of fluorescence closely overlapped with the voltage dependence of the gating charge movement. This analysis provides a clear demonstration that TMRM at this position experiences a local protein motion during voltage sensing.

We also observed fast ΔFs at some sites in the PD (Figure 1 and Table 1). The fast ΔFs in this region appear to primarily track the conformational changes of channel opening, rather than voltage sensing (see Figure S1A in the Supplemental Data available with this article online). These sites mapped to the tops of the turret and the S5-P loop of the PD (Figure S1B), rather than peripheral regions located closer to the VSD, which could potentially "feel" the voltage-sensing motion of S4. Taken together, these observations suggest that voltage-sensing motions do not propagate extensively into the extracellular portion of the PD but that opening rearrangements of the PD involve a conformational change that extends from the inner surface to the outer surface of the PD.

Magnitude of Protein Motion

Earlier evidence indicates that S4 substantially changes internal and external exposure during voltage sensing and carries most, if not all, of the gating charge (Gandhi and Isacoff, 2002), suggesting that it undergoes a large conformational change. In contrast, accessibility assays on S1 and S2 suggested that they do not posses a significant transmembrane motion (Gandhi et al., 2003; Ruta et al., 2005), although one charged residue on S2 has been suggested to move gating charge (Seoh et al.,

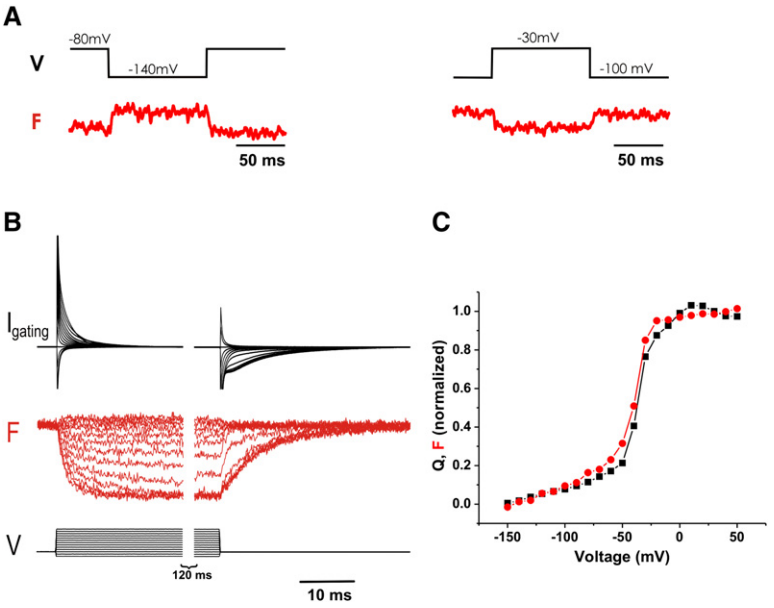

Figure 2. Fast ΔF in VSD Reports on Activation

(A) Fluorescence signals in response to a hyperpolarizing step (left) and a depolarizing step that does not open the channels (right) from TMRM attached to T276C. These channels open at ~−10 mV (data not shown).

(B) Gating currents (top) and fluorescence changes (middle) elicited from a site (I275C) that exhibits fast fluorescence changes in response to a family of voltage pulses (bottom). Holding potential is −80 mV, and the voltages steps range from −150 mV to +50 mV. Note the similarity in time course of gating currents and fluorescence changes.

(C) Normalized gating charge movement (black) and normalized steady-state fluorescence changes (red) show similar voltage-dependence properties. Points plotted are from data shown in part (B).

1996). The evidence has also been split as regards S3, with biotin trapping by Avidin in KvAP suggesting a large motion (Jiang et al., 2003b) but not in Shaker (Darman et al., 2006), and MTS reagent accessibility in Shaker (Gandhi et al., 2003; Gonzalez et al., 2005) and hanatoxin accessibility in Kv2.1 showing little change (Phillips et al., 2005).

We asked how we could extract information regarding the magnitude of protein motion from our fluorescence data set. The fluorescence changes we measure are due to changes in local environment experienced by the fluorophore during a conformational change in the protein. Any changes in local environment due to thermal fluctuations are averaged in the fluorescence signal, which arises from fluorophores attached to millions of channels at the plasma membrane of the cell. A ΔF in response to a voltage step means that the environment surrounding the fluorophore has changed beyond the average thermal fluctuations, due to a net rearrangement in the protein induced by voltage change. In other words, the conformational change in the protein must connect energetically separated states in order for us to see a fluorescence change. Large environmental transitions that would generate ΔFs of large magnitudes are possible with small protein movements. However, given side chain vibrations and the flexibility of some of the bonds in the TMRM linker, which will permit the TMRM to explore a cone of space, it is more likely that a larger motion will make for a larger environmental transition. In addition, very small protein movements connecting states that are energetically well separated (not visited by the protein just by simple thermal fluctuations) are possible but uncommon. Finally, in the event that a small motion causes a large environmental transition at one residue because it happens to carry that residue across a sharp structural boundary, we would observe a ΔF of large magnitude only at an isolated site, not at neighboring positions in the helix. Thus it is reasonable to assume that ΔFs of larger magnitudes observed at *several* residues in a helical segment are indicative of larger conformational changes of that segment. We reasoned that small motions of a helix would be expected to produce ΔFs of small magnitudes, perhaps only in a short segment of the helix at its edge of exposure, while large motions would produce large environment changes and ΔFs of large magnitudes that would be observed over a longer segment of the helix.

Starting with the outer end of each helical region of the Kv1.2 crystal structure, we counted the number of residues in each VSD helix that had a detectable ΔF. We found that the number of residues was smallest in S1 (with none of the residues showing detectable ΔFs falling within the helical region resolved in the Kv1.2 crystal structure), larger in S2, and largest in S3 and S4 (Figure 3A). We examined the ΔF amplitudes for each of the VSD helices (Figure 3B). The average fluorescence change progressively increased in magnitude from S1 to S4. The data are consistent with the notion that S3 and S4 undergo greater voltage-sensing motions than S1 and S2 (see Figure 6D below). Our results are consistent with an earlier perturbation scan of Kv2.1, which found a trend in perturbation energies across the VSD, with the smallest effects occurring in S1 and the largest effects occurring in S4 (Li-Smerin et al., 2000).

Nature of Voltage-Sensing Rearrangement of VSD

The large-magnitude ΔFs in S4 are consistent with the large changes in accessibility of S4 residues to MTS reagents (for review see Gandhi and Isacoff, 2002). However, the large magnitude of ΔFs in S3 were unexpected given the lack of change in accessibility of S3 residues to MTS reagents in Shaker (Darman et al., 2006; Gandhi et al., 2003). Could the ΔFs in S3 mean that S3 also

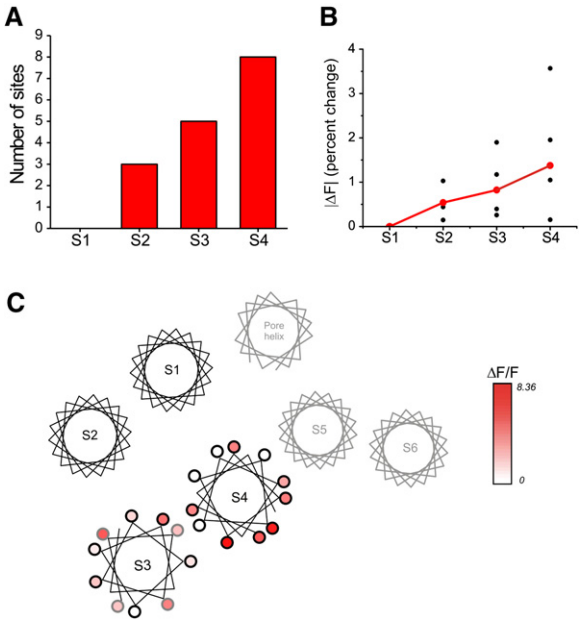

Figure 3. Pattern of ΔFs in the Voltage-Sensing Domain

(A) Number of fluorophore attachment positions from each helical region of the VSD of the Kv1.2 structure with a detectable ΔF. See Figure S6 for the sequence alignment used for S1 and S3 helices.

(B) Magnitude of the fast fluorescence components (ΔF) for the four helical segments of the voltage-sensing domain. The definition of helical segments is based on the crystal structure of the Kv1.2 channel, and alignments as discussed in Supplemental Experimental Procedures and shown in Figure S6. ΔF was computed as described in the Data Analysis section of Supplemental Experimental Procedures. Each black point represents a different site, and its value is the median ΔF of all cells tested for that site. The red points denote the mean of all sites for a given segment.

(C) Magnitude of fluorescence changes from S3 and S4 color coded according to the scale shown on the right and mapped onto a helical net diagram corresponding to a view of the channel's open-state model from the extracellular side of the membrane. Only the VSD of one subunit and the PD of its adjacent subunit are shown for clarity. S3 sites outlined in gray indicate sites that are not resolved in the Kv1.2 crystal structure but that are modeled as helical in the Rosetta-Membrane open-state model.

undergoes a large motion? In principle, large ΔFs in S3 could arise either from a motion of S3 itself or from the rearrangement of another part of the protein near S3, for example from the motion of S4. This would be predicted to occur only for attachment sites on the side of S3 that faces S4. However, the large ΔFs mapped to all sides of S3 (Figure 3C), suggesting that S3 moves relative to its entire surrounding environment during voltage sensing. These results are consistent with the biotin-trapping experiments in KvAP that showed a voltage-dependent change in both S3 and S4 access to a large avidin (Jiang et al., 2003b). In addition, the results suggest that the reason that S3 motion was not detected with MTS probing in Shaker (Gandhi et al., 2003) is that in the resting state of the VSD S3 is in a more external and exposed position compared to S4, perhaps at the outer end of the omega pathway (Tombola et al., 2007), and thus within reach of small MTS reagents. While S3 and S4 appear to move together, the large ΔFs seen along the interface between them (Figure 3C) suggest that they also experience a relative displacement.

Modeling of the Resting Conformation of the Kv1.2

We used the patterns of S3 and S4 motion observed in the fluorescence scan along with information about the resting-state conformation of the VSD gathered from a structure-driven perturbation scan of the omega current (Tombola et al., 2007) and accessibility of S6 residues (del Camino et al., 2005; del Camino and Yellen, 2001) to model the resting-state structure of Kv1.2 as described below. As a starting model, we used the previously developed Rosetta-Membrane model of Kv1.2 (Yarov-Yarovoy et al., 2006a).

Pore-Forming Domain and the S4-S5 Linker Modeling in the Resting State

To generate a model of the resting channel, we made a model of the closed state of the PD of the Kv1.2 channel that satisfies the data from Yellen and coworkers regarding the closed conformation of the intracellular gate (del Camino et al., 2005; del Camino and Yellen, 2001) (see Supplemental Experimental Procedures). Figure 4 shows our best model of the PD of Kv1.2 in the resting state. The pore is closed tightly by V410 (V478 in Shaker) side chains in the PD tetramer, and the V410 side chain is exposed to the water-accessible intracellular environment (Figures 4A and 4B). The S6 segment stays kinked at the conserved PVP-motif region in the resting state (Figures 4C and 4D). Comparison of our resting-state PD model with the Kv1.2 open-state structure (Long et al., 2005a) shows that the S6 closing movement involves a side movement of its intracellular part, which puts V410 and S6 residues downstream closer to the channel pore axis, so that the Cα atom of V410 moves ~5 Å between the open and closed states (Figures 4C and 4D).

We next modeled the resting-state position of the S4-S5 linker. The S4-S5 linker is proposed to interact specifically with S6 and to couple the voltage-dependent VSD movement to PD opening and closing (Lu et al., 2001, 2002). Maintaining the Kv1.2 open-state structure location of S4-S5 relative to S6 (Long et al., 2005a) (see Supplemental Experimental Procedures) and closing the gate, as we modeled above, results in a radial whole-body movement of S4-S5 by about 5–6 Å, which preserves its location between the hydrophobic and polar layers of the membrane. This movement of S4-S5 parallel to the plane of the membrane is significantly different from ~10 Å downward movement of the N-terminal end of the S4-S5 linker proposed earlier based on a KcsA-derived PD model of the closed state (Long et al., 2005b). To complete the resting-state PD model, we modeled the S5 region between S324 (S392 in Shaker) and V339 (V407 in Shaker) de novo using the Rosetta-Membrane method (Yarov-Yarovoy et al.,

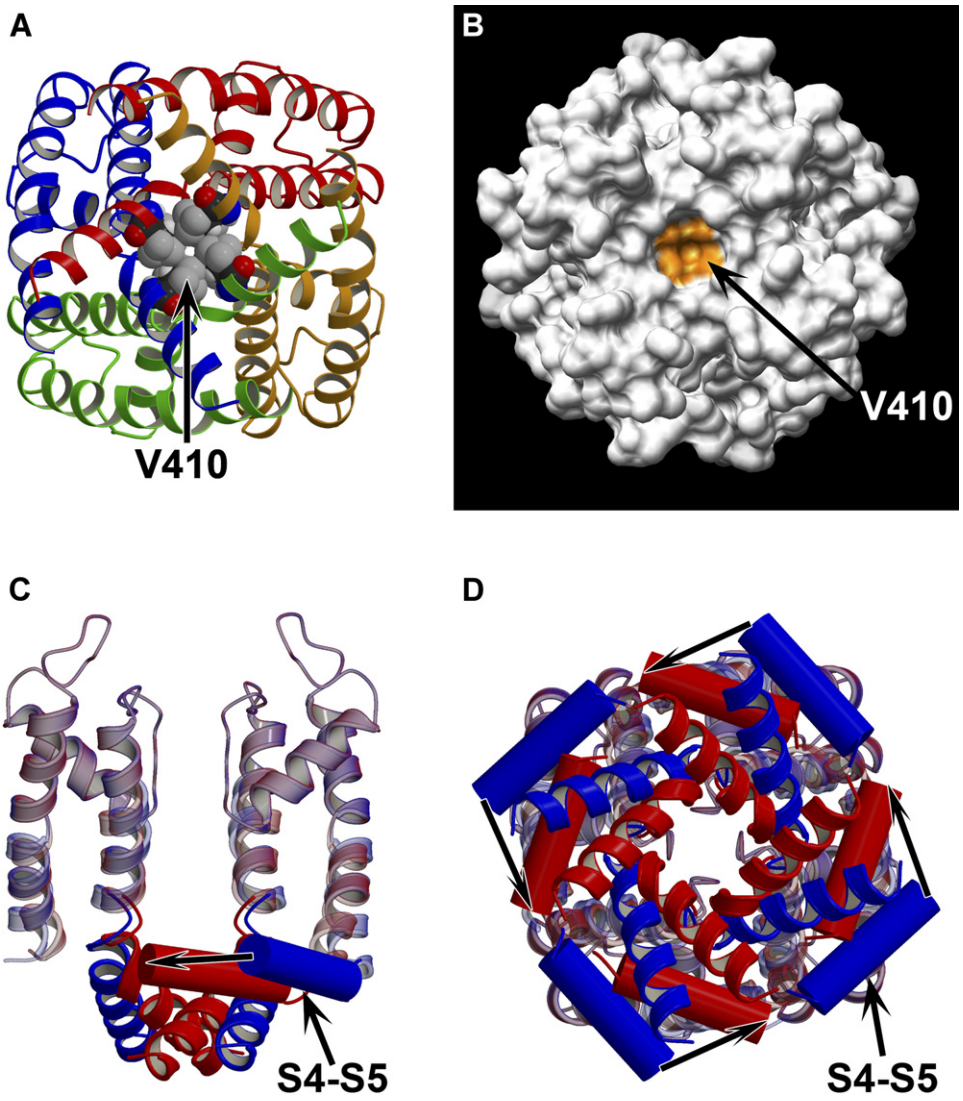

Figure 4. Resting-State Model of the PD and the S4-S5 Linker of the Kv1.2 Channel

(A) View from the intracellular side of the membrane of the ribbon representation of the PD model of Kv1.2 in the resting state. Side chains of V410 (V478 in Shaker) in S6 are shown in space-filling representation.

(B) View from the intracellular side of the membrane of the molecular surface representation of the PD of Kv1.2 in the resting state. Side chains of V410 are colored in orange.

(C) Side view of the cylinder representation of the S4-S5 linker and ribbon representation of the PD of the Kv1.2 in the resting (shown in red) and open (shown in blue) state superimposed over the selectivity filter residues. Only two opposing subunits forming the PD are shown for clarity.

(D) View of the models shown in (C) from the intracellular side of the membrane. All four subunits are shown. Panels (A), (C), and (D) were generated using Molscript (Kraulis, 1991) and Raster3D (Merritt and Bacon, 1997). Panel (B) was generated using Chimera (Pettersen et al., 2004; Sanner et al., 1996).

2006b). The model predicts that the intracellular part of S5 moves between the resting and open states, so that the N-terminal residue of S5 (M325 in Kv1.2; M393 in Shaker) is displaced by ~8 Å.

Voltage-Sensing Domain Modeling in the Resting State

We used the Rosetta-Membrane domain assembly method to build a resting-state model of the Kv1.2 VSD around our new resting-state model of the Kv1.2 PD (see Supplemental Experimental Procedures). The modeling was constrained by our fluorescence scan data in one way only. The fluorescence scan indicates that the outer half of S3 (S3b), S4, and the S3-S4 loop go through significant motion during voltage sensing. We therefore modeled these segments de novo in order to allow them to reorganize from their positions in the open state. Based on the omega current data (Tombola et al., 2007), we constrained the position of the extracellular end of S4 to be near the extracellular end of S5 and S6 from the adjacent

subunit and placed R1 in S4 (R294 in Kv1.2) close to E1 in S2 (E226 in Kv1.2).

We examined the ten largest clusters of models generated by the Rosetta-Membrane method, and the center model from the fourth largest cluster was selected as the best coarse-grained model based on the available experimental data (see Supplemental Experimental Procedures). An all-atom version of that model was subsequently generated with the high-resolution Rosetta-Membrane method (Barth et al., 2007) (see Supplemental Experimental Procedures). Figures 5A and 5B show our refined model of the Kv1.2 in the resting state. The model bears resemblance to earlier models (Chanda et al., 2005; Durell et al., 1998; Yarov-Yarovoy et al., 2006a), although the detailed positions of the VSD and PD segments differ (see Discussion). The S4 is tilted and positioned 3–5 Å further down, and the extracellular part of S3 is moved away from S1 and S2 compared to the earlier Kv1.2 resting-state model (Yarov-Yarovoy et al., 2006a). The first gating-charge-carrying arginine in S4 (R1), constrained to be near E1 in S2, forms a salt bridge with it (Figures 5C and 5D), placing R1 at the bottom of the extracellular water-accessible vestibule in the VSD, in agreement with data suggesting that this residue is accessible to *external* MTS reagents in the resting state (Larsson et al., 1996). The third gating-charge-carrying arginine (R3) and S308 in S4 (S376 in Shaker) face the intracellular water-accessible vestibule in the VSD (Figures 5C and D), in agreement with data suggesting that they are accessible to *internal* MTS reagents in the resting state (Larsson et al., 1996). The resting-state model accounts well for the omega scan data (Tombola et al., 2007): residues that had a "steric" effect on the amplitude of the omega current form a cluster in the core of the VSD, with A291 (A359 in Shaker) and R294 (R362 in Shaker) in S4 facing S1 and S2, while residues that had an "electrostatic" effect form a cluster near the extracellular end of S4 (Figure 6A).

Our open and closed models are in good agreement with experiments on the KvAP channel (Ruta et al., 2005). Mapping biotin-avidin accessibility data from KvAP onto our models shows that the location of the residues fits within 2–4 Å (Figure S2). The exception to this match is for the resting state at the intracellular end of S4, most likely due to a different tilt of the S4-S5 linker. In our resting-state model, it is positioned parallel to the plane of the membrane (see Results), while in KvAP there may be more of a tilt (for discussion see Supplemental Text). In addition, our resting-state model is compatible with recently reported disulfide bonding results (Campos et al., 2007), which suggested close proximity between Shaker's R1 (R362 in Shaker; R294 in Kv1.2) and one residue in S1 (I241 in Shaker; I177 in Kv1.2) and another in S2 (I287 in Shaker; I230 in Kv1.2). Our resting-state model shows that the homologous residues in Kv1.2 are within Cβ-Cβ distances observed between cysteines that are able to form disulfide bonds in flexible proteins (Careaga and Falke, 1992): with a distance from the Kv1.2 homolog of R1 (R294) of ~7 Å to I177 in S1 and ~11 Å to I230 in S2. Finally, our resting-state model is also compatible with the recent experimental analysis of the "down" state of KAT1 (Grabe et al., 2007) (though using a different sequence alignment than the one proposed by those authors, see Supplemental Text and Figure S3).

Agreement of the Resting-State Model with Fluorescence Data

A comparison between the open- and resting-state models shows significant difference between conformations of the extracellular part of S3 and S4, with a relative motion between the helices, consistent with the detection of ΔFs at the interface between them (Figures 3C and 6B). The averaged global movement for segments S1, S2, S3, and S4 was calculated from the displacement between the resting- and open-state models for every residue with a ΔF and was plotted in Figure 6D. The extent of global movement for each segment is strikingly similar to the patterns of fluorescence data reported for that segment (compare Figure 6D with Figures 3A and 3B).

Mapping the ΔF data onto the models (Figures 6B and 6C) reveals that in the open state the majority of positions with a large ΔF are exposed to the extracellular side of the membrane, while positions with small ΔFs are buried within the protein or lipid environment. For most residues in S3 and S4, the sign and amplitude of the ΔF correlates well with the sign and amplitude of the change in solvent-accessible surface area of the residue between the resting and open states (ΔSASA) (Figure 6E, red symbols). Negative ΔFs correlate with an increase in residue solvent-accessible surface area, and positive ΔFs correlate with a decrease in residue solvent-accessible surface area when Shaker Kv channel goes from the resting to open state. A few residues fell into a parallel outlying distribution (Figure 6E, gray symbols). Half of these residues are at the boundary between S3 and the S3-S4 linker, where the ΔF could be affected by a loop-to-helix transition from the resting-state model to the open-state model. The other half of the residues lie at the interface between S3 and S4, where the ΔF could be affected by rotation of S4 relative to S3.

DISCUSSION

Conformational Changes in the VSD during Gating

While X-ray crystal structures of the open state of the Kv channels have been obtained (Jiang et al., 2003a; Long et al., 2005a), the resting-state structure of these channels remains unknown. Several models have been proposed for the mechanism of voltage-dependent gating that drives channels between the resting/closed and activated/open states (Tombola et al., 2006). The "paddle" model suggests that S4 coupled to S3 moves 15–20 Å across the lipid bilayer (Jiang et al., 2003b; Ruta et al., 2005). The "helical screw" model suggests that S4 rotates and moves 3–13 Å across the lipid bilayer and that gating-charge-carrying arginines make sequential interactions with the negatively charged residues in the VSD during

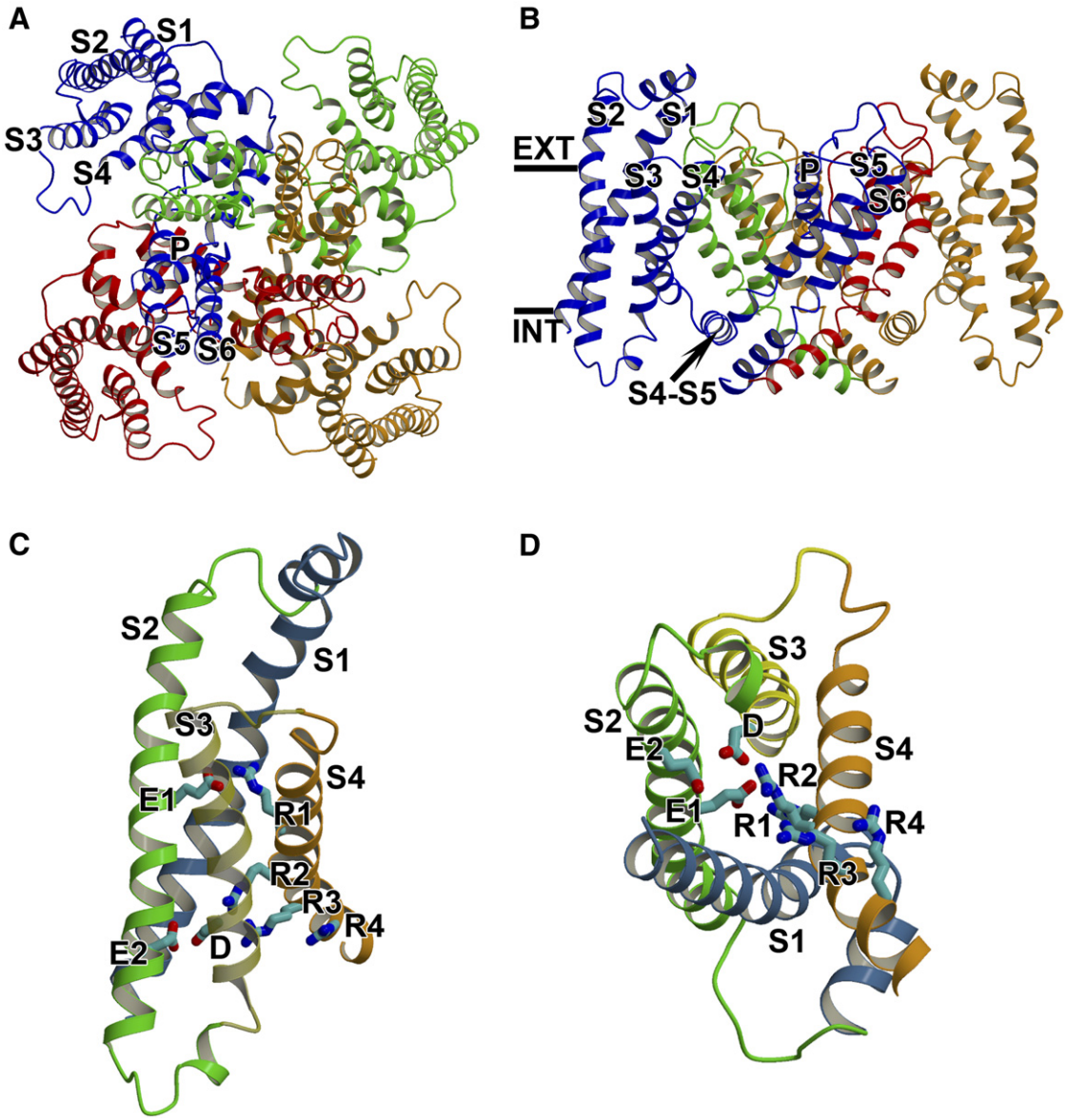

Figure 5. Resting-State Model of the VSD of the Kv1.2

(A) View of the ribbon representation of the Kv1.2 resting-state model from the extracellular side of the membrane. All four subunits are colored individually. Segments S1-S6 for blue colored subunit are labeled accordingly.

(B) View of the model shown in (A) from the side of the membrane. The VSD is shown only for blue and orange colored subunits for clarity. Segments S1-S6 and S4-S5 linker for blue colored subunit are labeled accordingly. Extracellular and intracellular edges of the membrane are marked by solid bars and labeled "EXT" and "INT," respectively.

(C) Side view of the VSD segments S1 through S4 only (colored individually) of the model shown in (A). Side chains of gating-charge-carrying arginines in S4 (labeled R1 through R4), E226 (E283 in Shaker, labeled E1) and E236 (E293 in Shaker, labeled E2) in S2, and D259 (D316 in Shaker, labeled D) in S3 shown in stick representation. Blue, red, and cyan colored atoms in the side chains shown represent nitrogen, oxygen, and carbon atoms, respectively.

(D) View of the model shown in (C) from the intracellular side of the membrane. The figure was generated using Molscript (Kraulis, 1991) and Raster3D (Merritt and Bacon, 1997).

the transition (Catterall, 1986; Gandhi and Isacoff, 2002; Guy and Seetharamulu, 1986; Lecar et al., 2003; Yarov-Yarovoy et al., 2006a). The "transporter" model suggests that S4 moves 2–4 Å across the lipid bilayer and that gating-charge-carrying arginines sense a transmembrane field focused by high dielectric aqueous crevices resulting from other conformational changes in the VSD (Chanda et al., 2005). Here, we use a combination of real-time fluorescence measurements of conformational changes and a variety of modeling approaches to build structural

models of the resting/closed and activated/open states of the Kv1.2 channel. Our models are compatible with many of the prior results and provide plausible explanations for the conformational changes underlying voltage sensing and for the mechanism by which changes in the VSD are propagated to the PD.

We carried out a large-scale fluorescence scan of the outer surface of the Shaker channel that revealed patterns of protein motion during the voltage-sensing transition. Large ΔFs observed along substantial lengths of S3 and S4 suggest a major coordinated rearrangement, as proposed in the paddle model. However, the environment changes detected at the interface between S3 and S4 indicate that these helices also move relative to one another, and not as a rigid body. Importantly, the majority of the S3 and S4 positions that were studied reported a very good correlation between the magnitude of the ΔF and magnitude of the change in residue environment (ΔSASA) (Figure 6E). This is especially striking because "per residue" information from the fluorescence scan was not used to constrain the modeling.

The pattern of ΔFs observed for residues on S1 and S2 suggests that these segments do not substantially change their environment during activation. For example, if S3 and S4 moved as proposed in the original paddle model, they would lie flush against S1 and S2 in the open state, but pivot/tilt down in the resting state. From the perspective of S1 and S2 there would be a transition on one surface of each helix from a proteinaceous environment to a lipid environment. In the transporter model, residues in S1 and S2 would be expected to face a protein-packed environment in one state and a large aqueous lake in the other. In both of these scenarios, residues on S1 and S2 would undergo a large environment change. In our models, the majority of the extracellularly accessible residues in S1 and S2 are separated from S3 and S4 by an aqueous environment in both the activated/open and resting/closed states, meaning that there is no great environment change. This is consistent with the small ΔFs observed at a small number of positions in S1 and S2. This is the first structural model that can explain the heterogeneity of ΔFs observed in the VSD.

Comparison of our refined Kv1.2 resting- and open-state models provides a view of the dominant conformational changes occurring in the voltage sensor upon gating (Figure 7A and Supplemental Movies). S4 moves as a tilting screw, rotating ~180° clockwise (when viewed from the extracellular side of the membrane), moving "up" vertically by 6–8 Å, and changing tilt angle from ~60° to ~35° in response to depolarization. The magnitude of the vertical motion in S4 varies from ~0 Å for S308 (S376 in Shaker) to ~14 Å for S289 (S357 in Shaker) and is estimated to be ~8 Å for R1 (R294 in Kv1.2; R362 in Shaker), ~10 Å for R2 (R297 in Kv1.2; R365 in Shaker), ~10 Å for R3 (R300 in Kv1.2; R368 in Shaker), and ~7 Å for R4 (R371 in Shaker) (see Table S1). Though this was not imposed as a constraint in the modeling, symmetry arises naturally concerning the position of the gating-charge-carrying arginines in the open and resting states with respect to the extracellular and intracellular edges of the membrane. In the open state, the distances from the extracellular edge of the 30 Å thick membrane are ~6 Å for R1, ~8 Å for R2, ~11 Å for R3, and ~16 Å for R4, while in the resting state the distances from the intracellular edge to the membrane are ~6 Å for R4, ~8 Å for R3, ~11 Å for R2, and ~15 Å for R1. This symmetry suggests that the most energetically optimal position of the S4 arginines in the open and resting state of the VSD is within the same distance from the extracellular and intracellular side of the membrane. S1, S2, and S3 move around S4 in a clockwise direction (viewed from the extracellular side of the membrane), as proposed earlier (Yarov-Yarovoy et al., 2006a). The screw motion of S4 agrees with earlier energy-transfer data on Shaker (Cha et al., 1999; Glauner et al., 1999) and prior sliding helix and helical screw models (Catterall, 1986; Durell et al., 1998; Guy and Seetharamulu, 1986). The magnitude of the vertical movement of S4 is compatible with how hanatoxin appears to partition into the membrane to bind the resting state of the VSD (Phillips et al., 2005) and with the estimate of the movement of the first gating-charge-carrying arginine through the membrane electric field (Ahern and Horn, 2005). Importantly, the magnitude of S4 movement is also compatible with previous data that appeared to be inconsistent. For instance, though the vertical translocation of S4 is larger than earlier distance estimates from energy transfer between donor-acceptor pairs of fluorophores (Chanda et al., 2005; Posson et al., 2005), the data is consistent once one takes into account the length and flexibility of linkers via which the fluorophores were attached (Tombola et al., 2006). Similarly, while the vertical movement in the current model is smaller than the 15–20 Å that was proposed based on the biotin-avidin accessibility data in KvAP (Jiang et al., 2003b; Ruta et al., 2005), a closer look indicates that the KvAP accessibility data maps well onto our open- and resting-state models of Kv1.2 (Figure S2), except at the inner end of S4, which may be less tilted in KvAP (Tombola et al., 2005a; Yarov-Yarovoy et al., 2006a).

The cumulative gating charge that is moved across the membrane electric field in the transition between our models of the resting and activated states is estimated to be ~14 elementary charges per channel (Figure 7B), close to the ~13 elementary charges estimated experimentally in Shaker (Aggarwal and MacKinnon, 1996; Seoh et al., 1996). The first four arginines in S4 contribute the most to the cumulative gating charge (Figure 7B), with the per subunit contribution being as follows: R1, 0.23*e*; R2, 0.61*e*; R3, 0.65*e*; and R4, 0.33*e*. This general conclusion agrees with earlier experimental work, although the values do not match the experimental values (Aggarwal and MacKinnon, 1996; Seoh et al., 1996) precisely. It should be noted that the contribution of R1 to the gating charge has not been clearly defined experimentally. Measurements of gating charge in neutralizing mutations led to estimates ranging from 0 and 1e, which were uncertain because of possible indirect effects on other gating

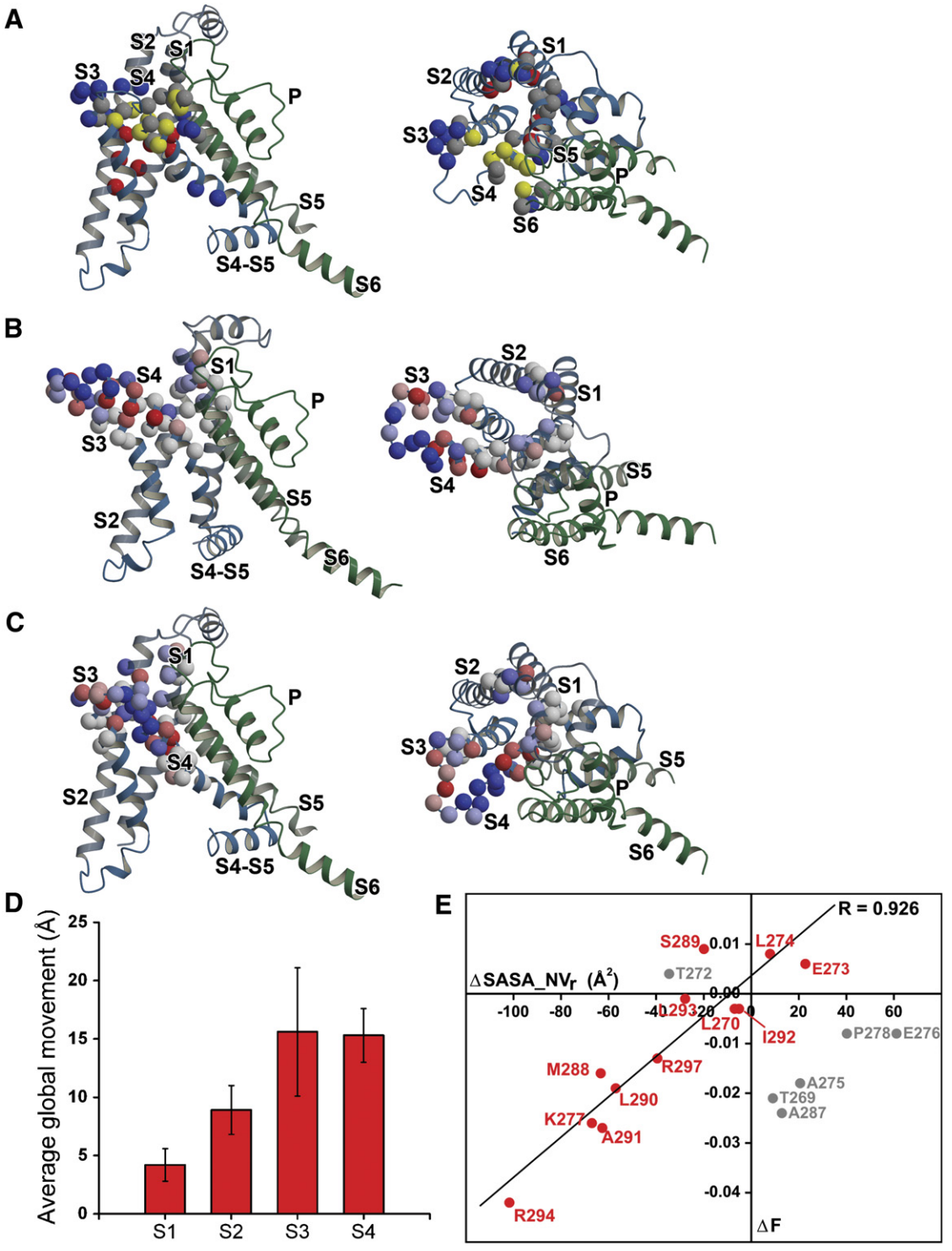

Figure 6. Experimental Data on Shaker Kv Channel Mapped onto the Refined Kv1.2 Resting-State Model

(A) Positions in the VSD and PD of the Shaker Kv channel studied by Tombola et al. (Tombola et al., 2007) mapped onto the ribbon representation of the Kv1.2 resting-state model. Only a single VSD from one subunit and PD from the adjacent subunit are shown from the side of the membrane (left panel) and extracellular side of the membrane (right panel). Segments S1-S6 and S4-S5 linker are labeled accordingly. Cα carbon atoms of the Kv1.2 residues corresponding to the Shaker Kv residues studied are shown as spheres and are colored based on their effect on the amplitude of the omega current as reported by Tombola et al. (Tombola et al., 2007) according to the following scheme: red, positions that had "steric" effect; yellow, positions that had "electrostatic" effect; blue, positions that had "null" effect; gray, positions that had "indirect" effect.

charges and complexities of more than one possible conducting state (Aggarwal and MacKinnon, 1996; Gandhi and Isacoff, 2002; Seoh et al., 1996). MTS accessibility analysis has suggested that R1 goes from being fully exposed to the extracellular environment in activated state to being in between the intracellular and extracellular environment in the resting state (Baker et al., 1998; Larsson et al., 1996; Yang et al., 1996), an interpretation supported by the observation that omega current flows in the resting state when R1 is substituted with a smaller uncharged side chain (Tombola et al., 2005b, 2007), suggesting transfer of ~0.5e. Given this broad range of experimental interpretations it is difficult to assess the validity of our estimate of ~0.25e gating charge contribution of R1 from our Kv1.2 channel models. This value was arrived at by simply turning off the R1 charge in the PB continuum electrostatic calculations without relaxing the atomic coordinates of the closed and open states. A more realistic approach would allow the structure to readjust following this change, as a real site-directed charge-neutralizing mutation affects not only the charge at that site but also the distribution of neighboring charges if they are mobile. The quantitative differences may also arise from inaccuracies in side chain packing by the structural modeling method (Yarov-Yarovoy et al., 2006a, 2006b).

It is particularly noteworthy that, without a focused transmembrane field, a much larger translocation of S4 would be required to account for the gating charge. High dielectric aqueous regions contribute to focus the transmembrane field in both the open and closed conformation, thereby controlling the magnitude of the gating charge. In the open state, the field is focused toward the extracellular half of the membrane by the large central vestibule at the intracellular pore entrance. In the closed state, the field is again focused toward the extracellular half of the membrane, this time by the wide aqueous crevice that opens up at the center of the VSD under the tilted S4 helix. The existence of the latter had been deduced indirectly from experiments (Ahern and Horn, 2005; Chanda et al., 2005; Islas and Sigworth, 2001; Starace and Bezanilla, 2004; Tombola et al., 2007).

Molecular Model of the Voltage-Dependent Gating of Kv Channels

Comparison of our resting-state model to the Kv1.2 open-state model (Long et al., 2005a) suggest a molecular mechanism of the voltage-dependent gating of Kv channels. The data available to date suggest that voltage-dependent gating involves two major sets of conformational change during the transition between the resting/closed and activated/open state: independent motions of the VSDs with transfer of most of the gating charge between the resting state and an activated-not-open state that keeps the intracellular PD gate closed (Bezanilla et al., 1994; del Camino et al., 2005; Horn et al., 2000; Ledwell and Aldrich, 1999; Pathak et al., 2005; Perozo et al., 1994; Schoppa and Sigworth, 1998; Soler-Llavina et al., 2006), and a concerted opening transition of the VSD and PD, which transfers a minor component of the gating charge between the activated-not-open state and the state that opens the intracellular PD gate for ion conduction (del Camino et al., 2005; Mannuzzu and Isacoff, 2000; Pathak et al., 2005; Schoppa and Sigworth, 1998; Smith-Maxwell et al., 1998a; Smith-Maxwell et al., 1998b; Soler-Llavina et al., 2006; Zagotta et al., 1994). The activated-not-open state is stabilized by S4's ILT residues (V369I, I372L, and S376T in Shaker; V301I, I304L, and S308T in Kv1.2) (Ledwell and Aldrich, 1999; Smith-Maxwell et al., 1998a, 1998b), which map on to one face of the S4 helix and have been proposed to face the neighboring subunit's S5 (Pathak et al., 2005). Complementary to this, a cluster of residues on the intracellular half of S5, which plays a role in the concerted gating transition, has been proposed to interact with the ILT residues (Soler-Llavina et al., 2006).

In our resting-state model, the ILT residues point from S4 into the intracellular water-accessible vestibule within the VSD and away from the S5 cluster (Figure 7C). The 180° turn and upward displacement of S4 would bring the ILT residues into contact with the S5 cluster if there were little or no motion in the PD. We propose this to represent the independent transition in the VSD from the resting to the active-not-open state. In our model, for the

(B and C) Positions in the VSD and PD of the Shaker Kv channel studied in the fluorescence scan (Table 1) mapped onto the ribbon representation of the Kv1.2 open-state (B) and resting-state (C) models. Only a single VSD from one subunit and PD from the adjacent subunit are shown from the side of the membrane (left panel) and extracellular side of the membrane (right panel). Segments S1-S6 and S4-S5 linker are labeled accordingly. Cα carbon atoms of the Kv1.2 residues corresponding to the Shaker Kv residues studied are shown as spheres and are colored based on a sign of fluorescence change (ΔF) reported in Table 1 according to the following scheme: red, positions that reported $\Delta F < -0.03$; red to white, positions that reported $-0.03 < \Delta F < 0$; white, positions that reported $\Delta F = 0$; white to blue, positions that reported $0 < \Delta F < 0.03$; blue, positions that reported $\Delta F > 0.03$.

(D) Amplitude of average global movement between the resting and open states of the VSD residues studied for each VSD segment. Global movement of each VSD segment was calculated from an average difference in position of Cα atoms of VSD residues studied in the Kv1.2 between the resting (closed) and activated (open) state models superimposed over Cα atom positions of GYG residues in the selectivity filter (G376, Y377, and G378 in the Kv1.2; G444, Y445, and G446 in Shaker). Error bars represent standard deviation.

(E) Change in the amplitude of the fast fluorescence (ΔF) for the S3 and S4 residues only plotted versus change in residue solvent-accessible surface area between the resting and open states normalized to the ratio of TMRM volume to residue side chain volume at each position studied ($\Delta SASA\_NV_r$) (see Supplemental Experimental Procedures). The red points represent the S3 and S4 residues that are not forming a part of the S3-S4 loop and are not at the interface between the S3 and S4 in either the resting or closed state. The gray points represent the S3 and S4 residues that are forming a part of the S3-S4 loop or are at the interface between the S3 and S4 in either resting or closed state. The linear regression fit is plotted for the red points only.

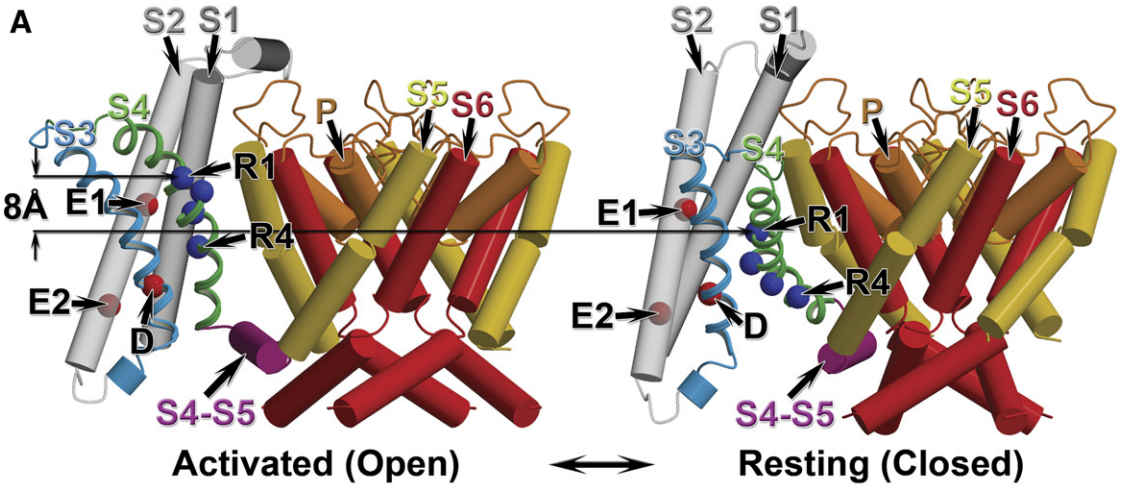

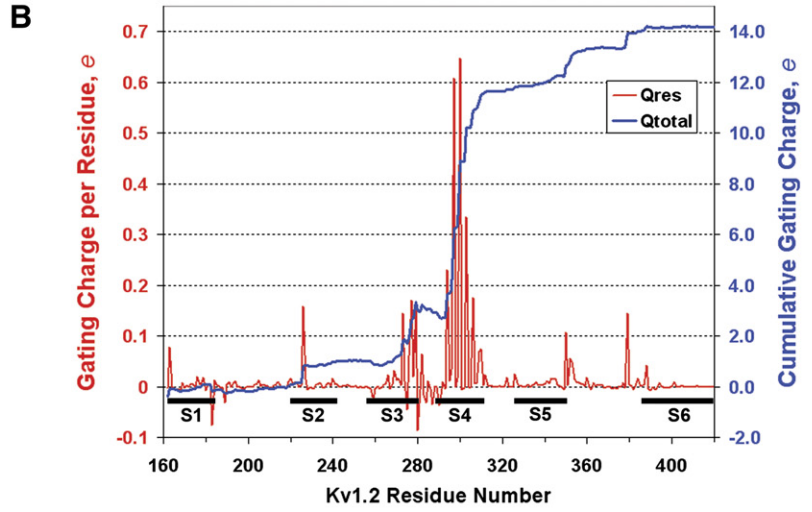

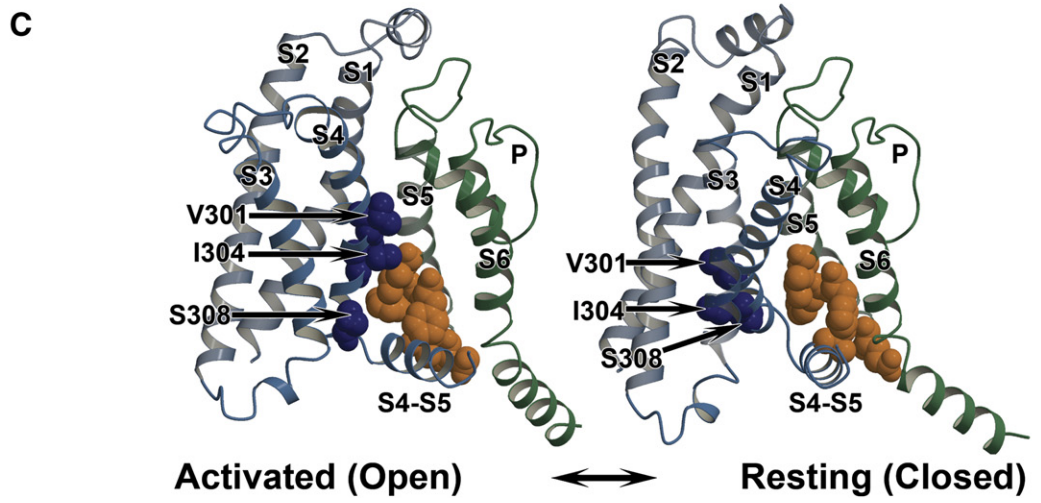

Figure 7. Comparison of the Kv1.2 Models of the Activated (Open) and Resting (Closed) States

(A) View of the cylinder representation of the Kv1.2 open-state (left panel) and resting-state (right panel) models. Only a single VSD is shown attached to a tetramer of the PD for clarity. Transmembrane segments S1 and S2 are colored gray, and segments S3 through S6 and the P loop are colored by

intracellular half of S6 to swing and open the gate, S5 must first tilt its intracellular end by ~7 Å tangentially around the PD. Thus, we propose that the second major activation rearrangement involves tilting of S4 coupled to tilting of the intracellular half of the adjacent S5. This counterclockwise movement (viewed from the extracellular side of the membrane) would enable the S4-S5 linker and S6 in all four subunits to move together and open the intracellular gate of the pore.

Recent studies suggested a role of lipid phosphate groups in Kv channel gating, including interaction with S4 arginines (Ramu et al., 2006; Schmidt et al., 2006). Our resting-state model, in which the arginines are shielded from the hydrocarbon core of the membrane by S1, S2, and S3, does not suggest interaction of the S4 arginines with lipid phosphate groups. Furthermore, during the rotational and translational movement of S4 between the resting and active-not-open conformations, the S4 arginines would still be oriented toward S1, S2, and S3 and away from the membrane (see Figure 7A and the Supplemental Movies). However, the final opening transition may place the first two arginines in contact with the extracellular lipid phosphate groups (Long et al., 2005b). This is consistent with the observation that KvAP cannot be activated in the absence of the negatively charged phospholipids (Schmidt et al., 2006), perhaps because lacking the stabilization provided by the interaction of the arginines with the lipid phosphate groups in the open state, it remains stuck in the activated-not-open conformation. Further experiments are necessary to test this hypothesis and to try to understand whether interactions between S4 arginines and lipid phosphate groups drive S4 tilt, and thus lead to the concerted opening transition of the PD.

Comparison to Other Structural Models of Kv Channels

Recently, several structural models of the open and resting state of the Kv channels have been proposed (Chanda et al., 2005; Durell et al., 2004; Grabe et al., 2007; Tombola et al., 2007; Yarov-Yarovoy et al., 2006a). In addition, a conceptual model of the KvAP resting state was proposed in the paddle model of gating (Jiang et al., 2003b; Ruta et al., 2005). Our open- and resting-state Kv channel models suggest the following new details of the molecular mechanism of the voltage-dependent gating: (1) S4 moves vertically by about 6–8 Å (see Figure 7A and the Supplemental Movies). Previously published complete structural models of the transmembrane region of the VSD in the open and/or closed states suggested significantly different magnitudes of the S4 vertical movement: ~2–4 Å (Chanda et al., 2005), ~3 Å (Yarov-Yarovoy et al., 2006a), and 10–13 Å (Durell et al., 2004; Grabe et al., 2007; Tombola et al., 2007). The previously published conceptual model of the KvAP resting state (Jiang et al., 2003b; Ruta et al., 2005) suggested ~15–20 Å vertical movement of the S4; (2) S3 moves relative to S1, S2, and S4 (Figure 7A and the Supplemental Movies). None of the previously published complete structural models suggested significant movement of the S3 relative to all the other VSD segments; (3) concerted movement of the S4, S5, S4-S5 linker, and S6 of all four subunits in the opening transition (see Discussion and the Supplemental Movies). None of the previously published complete structural models of Kv channels suggested such a mechanism of the concerted opening transition. Despite the differences with the earlier models, we have shown that our models can account for much of the seemingly disparate earlier data that led to those divergent models, that it can uniquely account for our new fluorescence data, that it agrees, grosso modo, with what is known about gating charge contribution, and that it leads to a coherent mechanism by which voltage sensing is coupled to gating.

In conclusion, the movement underlying the gating mechanism emerging from the present analysis retains features of the three principal models proposed previously. The magnitude of S4 vertical movement is compatible with the earlier data and is ~6–8 Å larger than in the transporter model (2–4 Å), but smaller than in the paddle model (15–20 Å). As pictured in the helical screw model (Catterall, 1986; Guy and Seetharamulu, 1986), the predominant movement is an axial rotation of S4 by ~180°. As in the transporter model (Chanda et al., 2005), high dielectric crevices contribute to focus the transmembrane field, thus increasing the gating charge that couples energetically the VSD to the membrane voltage. As emphasized in the paddle model (Jiang et al., 2003b), the S4 segment is partially exposed to the lipid environment; however, the S4 gating charges move through a "virtual

a rainbow scheme from blue to red. The S4-S5 linker is colored purple. Positions of Cα carbon atoms of the gating-charge-carrying arginines in S4 (labeled as R1 and R4 and colored in blue), E226 in S2 (E283 in Shaker; labeled as E1 and colored in red) and E236 in S2 (E293 in Shaker; labeled as E2 and colored in red), and D259 in S3 (D316 in Shaker; labeled D and colored red) are shown in sphere representation. Vertical translation of the first gating-charge-carrying arginine (R1) between the activated (open) and resting (closed) states along the membrane normal vector is indicated by arrows. The S3 and S4 are shown in ribbon representation. Segments S1-S6 and the P loop for one subunit are labeled accordingly.

(B) Cumulative gating charge in a tetramer (blue) and gating charge per residue in a single subunit (red) transferred across the membrane electric field between the resting to open state plotted as a function of Kv1.2 residue position.

(C) View of the ribbon representation of the Kv1.2 open state (left panel) and resting state (right panel) models of the VSD from one subunit and the PD from the adjacent subunit from the side of the membrane. Segments S1-S6 and the S4-S5 linker are labeled accordingly. Positions in the Shaker Kv channel studied by Soler-Llavina et al. (Soler-Llavina et al., 2006) mapped onto the Kv1.2 open-state structure (Long et al., 2005a) and Kv1.2 resting-state model. The Kv1.2 residues corresponding to the ILT triple mutant (Ledwell and Aldrich, 1999; Smith-Maxwell et al., 1998a; Smith-Maxwell et al., 1998b) (colored in dark blue) and intracellular cluster of the S5 residues studied by Soler-Llavina et al. (Soler-Llavina et al., 2006) (colored in orange) are shown in space-filling representation. Residue numbers in the ILT triple mutant positions correspond to the Kv1.2 channel sequence. The figure was generated using Molscript (Kraulis, 1991) and Raster3D (Merritt and Bacon, 1997).

gating pore" within the VSD, without being exposed directly to the nonpolar hydrocarbon core of the membrane. The compatibility of our Kv channel models with a wide body of data, a good deal of which had been previously thought to be contradictory, appears to resolve the controversy about the magnitude and character of the movement underlying voltage gating.

EXPERIMENTAL PROCEDURES

For detailed Experimental Procedures, please refer to the Supplemental Data.

Fluorescence Recordings

Procedures for site-directed mutagenesis, in vitro transcriptions, RNA injections, oocyte preparation and injections, and labeling by TMRM were performed as described previously (Gandhi et al., 2000; Pathak et al., 2005). Two-electrode voltage-clamp fluorometry was performed 1–2 days after oocyte injection as described in Mannuzzu et al. (1996), in bath solution composed of (in mM): 110 NaMES, 2 KMES, 2 $CaMES_2$, and 10 HEPES (pH 7.5) or 20 NaMES, 90 KMES, 2 $CaMES_2$, and 10 HEPES (pH 7.5).

Data Analysis

Data analysis was done with the Axon Laboratory programs pClamp8 and Clampfit 9.2 (Axon Instruments) and custom-prepared Matlab programs as described in the Supplemental Experimental Procedures. Each fluorescence trace was baseline subtracted and bleach corrected. The fluorescence response to the depolarizing step was fit by a double-exponential function. The two components of the fit correspond to channel activation and slow inactivation (see Results). The amplitude of the fit to the activation component (represented as ΔF) was averaged across cells for a given site. ΔF values correspond to the conventionally used representation $\Delta F/F$ and are expressed as percent changes (Table 1).

Modeling of the Kv1.2 Channel

The Rosetta-Membrane method (Yarov-Yarovoy et al., 2006b; Barth et al., 2007) and the CHARMM program (Brooks et al., 1983) were used to model the Kv1.2 channel in the resting and activated-open states as described in the Supplemental Experimental Procedures. Coordinates of the Kv1.2 channel models are available in the Supplemental Data.

Supplemental Data

The Supplemental Data for this article can be found online at http://www.neuron.org/cgi/content/full/56/1/124/DC1/.

ACKNOWLEDGMENTS

We gratefully acknowledge Lisa Kurtz for invaluable help with molecular biology and preliminary data collection; Sandra Wiese for excellent molecular biology assistance; Chris Gandhi, David Baker, Jacqui Gulbis, and William A. Catterall for many helpful discussions; and Laura Gonzalez for making the movies. This work was supported by NIH Grant R01NS035549 (to E.Y.I.), NIMH Career Development Research Grant K01 MH67625 (to V.Y.-Y.), an American Heart Association postdoctoral fellowship (to F.T.), and NIH Grant GM-62342 (to B.R.). In addition, V.Y.-Y.'s work was supported in part by NIH Grant R01 NS15751 (to William A. Catterall).

M.M.P. and E.Y.I. designed the fluorescence scan; M.M.P. performed fluorescence experiments with assistance from S.K.; M.M.P. and G.A. analyzed fluorescence data. V.Y.-Y. designed and performed the Rosetta-Membrane modeling; B.R. performed molecular dynamics simulations and gating charge calculations; P.B. performed full atom refinement of the Kv1.2 structural models. V.Y.-Y., F.T., M.M.P., B.R., and E.Y.I. all contributed to data interpretation and modeling. V.Y.-Y., M.M.P., and E.Y.I. wrote the manuscript. All authors discussed the results and commented on the manuscript.

Received: May 14, 2007
Revised: August 14, 2007
Accepted: September 18, 2007
Published: October 3, 2007

REFERENCES

Aggarwal, S.K., and MacKinnon, R. (1996). Contribution of the S4 segment to gating charge in the Shaker K+ channel. Neuron *16*, 1169–1177.

Ahern, C.A., and Horn, R. (2005). Focused electric field across the voltage sensor of potassium channels. Neuron *48*, 25–29.

Baker, O.S., Larsson, H.P., Mannuzzu, L.M., and Isacoff, E.Y. (1998). Three transmembrane conformations and sequence-dependent displacement of the S4 domain in shaker K+ channel gating. Neuron *20*, 1283–1294.

Barth, P., Schonbrun, J., and Baker, D. (2007). Efficient all-atom modeling of interactions, structural specificities and helical distortions in membrane proteins. Proc. Natl. Acad. Sci. USA, in press.

Bezanilla, F., Perozo, E., and Stefani, E. (1994). Gating of Shaker K+ channels: II. The components of gating currents and a model of channel activation. Biophys. J. *66*, 1011–1021.

Brooks, B.R., Bruccoleri, R.E., Olafson, B.D., States, D.J., Swaminathan, S., and Karplus, M. (1983). CHARMM: A program for macromolecular energy minimization and dynamics calculations. J. Comp. Chem. *4*, 187–217.

Campos, F.V., Chanda, B., Roux, B., and Bezanilla, F. (2007). Two atomic constraints unambiguously position the S4 segment relative to S1 and S2 segments in the closed state of Shaker K channel. Proc. Natl. Acad. Sci. USA *104*, 7904–7909.

Careaga, C.L., and Falke, J.J. (1992). Thermal motions of surface alpha-helices in the D-galactose chemosensory receptor. Detection by disulfide trapping. J. Mol. Biol. *226*, 1219–1235.

Catterall, W.A. (1986). Voltage-dependent gating of sodium channels: Correlating structure and function. Trends Neurosci. *9*, 7–10.

Cha, A., and Bezanilla, F. (1997). Characterizing voltage-dependent conformational changes in the Shaker K+ channel with fluorescence. Neuron *19*, 1127–1140.

Cha, A., Snyder, G.E., Selvin, P.R., and Bezanilla, F. (1999). Atomic scale movement of the voltage-sensing region in a potassium channel measured via spectroscopy. Nature *402*, 809–813.

Chanda, B., Asamoah, O.K., Blunck, R., Roux, B., and Bezanilla, F. (2005). Gating charge displacement in voltage-gated ion channels involves limited transmembrane movement. Nature *436*, 852–856.

Darman, R.B., Ivy, A.A., Ketty, V., and Blaustein, R.O. (2006). Constraints on voltage sensor movement in the shaker K+ channel. J. Gen. Physiol. *128*, 687–699.

del Camino, D., and Yellen, G. (2001). Tight steric closure at the intracellular activation gate of a voltage-gated K(+) channel. Neuron *32*, 649–656.

del Camino, D., Kanevsky, M., and Yellen, G. (2005). Status of the intracellular gate in the activated-not-open state of shaker K+ channels. J. Gen. Physiol. *126*, 419–428.

Durell, S.R., Hao, Y., and Guy, H.R. (1998). Structural models of the transmembrane region of voltage-gated and other K+ channels in open, closed, and inactivated conformations. J. Struct. Biol. *121*, 263–284.

Durell, S.R., Shrivastava, I.H., and Guy, H.R. (2004). Models of the structure and voltage-gating mechanism of the shaker K+ channel. Biophys. J. *87*, 2116–2130.

Gandhi, C.S., and Isacoff, E.Y. (2002). Molecular models of voltage sensing. J. Gen. Physiol. *120*, 455–463.

Gandhi, C.S., Loots, E., and Isacoff, E.Y. (2000). Reconstructing voltage sensor-pore interaction from a fluorescence scan of a voltage-gated K+ channel. Neuron *27*, 585–595.

Gandhi, C.S., Clark, E., Loots, E., Pralle, A., and Isacoff, E.Y. (2003). The orientation and molecular movement of a k(+) channel voltage-sensing domain. Neuron *40*, 515–525.

Glauner, K.S., Mannuzzu, L.M., Gandhi, C.S., and Isacoff, E.Y. (1999). Spectroscopic mapping of voltage sensor movement in the Shaker potassium channel. Nature *402*, 813–817.

Gonzalez, C., Morera, F.J., Rosenmann, E., Alvarez, O., and Latorre, R. (2005). S3b amino acid residues do not shuttle across the bilayer in voltage-dependent Shaker K+ channels. Proc. Natl. Acad. Sci. USA *102*, 5020–5025.

Grabe, M., Lai, H.C., Jain, M., Nung Jan, Y., and Yeh Jan, L. (2007). Structure prediction for the down state of a potassium channel voltage sensor. Nature *445*, 550–553.

Guy, H.R., and Seetharamulu, P. (1986). Molecular model of the action potential sodium channel. Proc. Natl. Acad. Sci. USA *83*, 508–512.

Horn, R., Ding, S., and Gruber, H.J. (2000). Immobilizing the moving parts of voltage-gated ion channels. J. Gen. Physiol. *116*, 461–476.

Islas, L.D., and Sigworth, F.J. (2001). Electrostatics and the gating pore of Shaker potassium channels. J. Gen. Physiol. *117*, 69–89.

Jiang, Y., Lee, A., Chen, J., Ruta, V., Cadene, M., Chait, B.T., and MacKinnon, R. (2003a). X-ray structure of a voltage-dependent K+ channel. Nature *423*, 33–41.

Jiang, Y., Ruta, V., Chen, J., Lee, A., and MacKinnon, R. (2003b). The principle of gating charge movement in a voltage-dependent K+ channel. Nature *423*, 42–48.

Kraulis, P.J. (1991). MOLSCRIPT: a program to produce both detailed and schematic plots of protein structures. J. Appl. Cryst. *24*, 946–950.

Larsson, H.P., Baker, O.S., Dhillon, D.S., and Isacoff, E.Y. (1996). Transmembrane movement of the shaker K+ channel S4. Neuron *16*, 387–397.

Lecar, H., Larsson, H.P., and Grabe, M. (2003). Electrostatic model of S4 motion in voltage-gated ion channels. Biophys. J. *85*, 2854–2864.

Ledwell, J.L., and Aldrich, R.W. (1999). Mutations in the S4 region isolate the final voltage-dependent cooperative step in potassium channel activation. J. Gen. Physiol. *113*, 389–414.

Lee, S.Y., Lee, A., Chen, J., and MacKinnon, R. (2005). Structure of the KvAP voltage-dependent K+ channel and its dependence on the lipid membrane. Proc. Natl. Acad. Sci. USA *102*, 15441–15446.

Li-Smerin, Y., Hackos, D.H., and Swartz, K.J. (2000). α-helical structural elements within the voltage-sensing domains of a K(+) channel. J. Gen. Physiol. *115*, 33–50.

Long, S.B., Campbell, E.B., and Mackinnon, R. (2005a). Crystal structure of a mammalian voltage-dependent Shaker family K+ channel. Science *309*, 897–903.

Long, S.B., Campbell, E.B., and Mackinnon, R. (2005b). Voltage sensor of Kv1.2: structural basis of electromechanical coupling. Science *309*, 903–908.

Lu, Z., Klem, A.M., and Ramu, Y. (2001). Ion conduction pore is conserved among potassium channels. Nature *413*, 809–813.

Lu, Z., Klem, A.M., and Ramu, Y. (2002). Coupling between voltage sensors and activation gate in voltage-gated K+ channels. J. Gen. Physiol. *120*, 663–676.

Mannuzzu, L.M., and Isacoff, E.Y. (2000). Independence and cooperativity in rearrangements of a potassium channel voltage sensor revealed by single subunit fluorescence. J. Gen. Physiol. *115*, 257–268.

Mannuzzu, L.M., Moronne, M.M., and Isacoff, E.Y. (1996). Direct physical measure of conformational rearrangement underlying potassium channel gating. Science *271*, 213–216.

Merritt, E.A., and Bacon, D.J. (1997). Raster3D: Photorealistic molecular graphics. Methods Enzymol. *277*, 505–524.

Pathak, M., Kurtz, L., Tombola, F., and Isacoff, E. (2005). The cooperative voltage sensor motion that gates a potassium channel. J. Gen. Physiol. *125*, 57–69.

Perozo, E., Santacruz-Toloza, L., Stefani, E., Bezanilla, F., and Papazian, D.M. (1994). S4 mutations alter gating currents of Shaker K channels. Biophys. J. *66*, 345–354.

Pettersen, E.F., Goddard, T.D., Huang, C.C., Couch, G.S., Greenblatt, D.M., Meng, E.C., and Ferrin, T.E. (2004). UCSF Chimera—a visualization system for exploratory research and analysis. J. Comput. Chem. *25*, 1605–1612.

Phillips, L.R., Milescu, M., Li-Smerin, Y., Mindell, J.A., Kim, J.I., and Swartz, K.J. (2005). Voltage-sensor activation with a tarantula toxin as cargo. Nature *436*, 857–860.

Posson, D.J., Ge, P., Miller, C., Bezanilla, F., and Selvin, P.R. (2005). Small vertical movement of a K+ channel voltage sensor measured with luminescence energy transfer. Nature *436*, 848–851.

Ramu, Y., Xu, Y., and Lu, Z. (2006). Enzymatic activation of voltage-gated potassium channels. Nature *442*, 696–699.

Ruta, V., Chen, J., and MacKinnon, R. (2005). Calibrated measurement of gating-charge arginine displacement in the KvAP voltage-dependent K+ channel. Cell *123*, 463–475.

Sanner, M.F., Olson, A.J., and Spehner, J.C. (1996). Reduced surface: an efficient way to compute molecular surfaces. Biopolymers *38*, 305–320.

Schmidt, D., Jiang, Q.X., and MacKinnon, R. (2006). Phospholipids and the origin of cationic gating charges in voltage sensors. Nature *444*, 775–779.

Schoppa, N.E., and Sigworth, F.J. (1998). Activation of Shaker potassium channels. III. An activation gating model for wild-type and V2 mutant channels. J. Gen. Physiol. *111*, 313–342.

Seoh, S.A., Sigg, D., Papazian, D.M., and Bezanilla, F. (1996). Voltage-sensing residues in the S2 and S4 segments of the Shaker K+ channel. Neuron *16*, 1159–1167.

Smith-Maxwell, C.J., Ledwell, J.L., and Aldrich, R.W. (1998a). Role of the S4 in cooperativity of voltage-dependent potassium channel activation. J. Gen. Physiol. *111*, 399–420.

Smith-Maxwell, C.J., Ledwell, J.L., and Aldrich, R.W. (1998b). Uncharged S4 residues and cooperativity in voltage-dependent potassium channel activation. J. Gen. Physiol. *111*, 421–439.

Soler-Llavina, G.J., Chang, T.H., and Swartz, K.J. (2006). Functional interactions at the interface between voltage-sensing and pore domains in the Shaker K(v) channel. Neuron *52*, 623–634.

Starace, D.M., and Bezanilla, F. (2004). A proton pore in a potassium channel voltage sensor reveals a focused electric field. Nature *427*, 548–553.

Tombola, F., Pathak, M.M., and Isacoff, E.Y. (2005a). How far will you go to sense voltage? Neuron *48*, 719–725.

Tombola, F., Pathak, M.M., and Isacoff, E.Y. (2005b). Voltage-sensing arginines in a potassium channel permeate and occlude cation-selective pores. Neuron *45*, 379–388.

Tombola, F., Pathak, M.M., and Isacoff, E.Y. (2006). How does voltage open an ion channel? Annu. Rev. Cell Dev. Biol. *22*, 23–52.

Tombola, F., Pathak, M.M., Gorostiza, P., and Isacoff, E.Y. (2007). The twisted ion-permeation pathway of a resting voltage-sensing domain. Nature *445*, 546–549.

Yang, N., George, A.L., Jr., and Horn, R. (1996). Molecular basis of charge movement in voltage-gated sodium channels. Neuron *16*, 113–122.

Yarov-Yarovoy, V., Baker, D., and Catterall, W.A. (2006a). Voltage sensor conformations in the open and closed states in ROSETTA structural models of K(+) channels. Proc. Natl. Acad. Sci. USA *103*, 7292–7297.

Yarov-Yarovoy, V., Schonbrun, J., and Baker, D. (2006b). Multipass membrane protein structure prediction using Rosetta. Proteins *62*, 1010–1025.

Zagotta, W.N., Hoshi, T., and Aldrich, R.W. (1994). Shaker potassium channel gating. III: Evaluation of kinetic models for activation. J. Gen. Physiol. *103*, 321–362.